Nuclear Instruments and Methods in Physics Research A329 (1993) 112–116
North-Holland

NUCLEAR
INSTRUMENTS
& METHODS
IN PHYSICS
RESEARCH
Section A

On the cross calibration of calorimeters at ep colliders

J. Blümlein and M. Klein
DESY-Institut für Hochenergiephysik, O-1615 Zeuthen, Germany

Received 10 November 1992

It is demonstrated that the comparison of cross sections measured in inclusive deep inelastic electron–proton scattering with electrons and hadrons only can be utilized to recognize or even determine the size of absolute energy miscalibration of electromagnetic and hadronic calorimeters. The method is illustrated for the case of the HERA detector H1.

1. Introduction

The kinematical variables in inclusive deep inelastic neutral current electron–proton scattering, $ep \to eX$, can be determined by measuring the angle and energy either of the outgoing electron or of the current jet. The detectors H1 and ZEUS at the electron–proton accelerator HERA are equipped with huge calorimeter systems in order to measure the electromagnetic and hadronic energies with resolutions of the order of $\sim 20\%/\sqrt{E'_e/\mathrm{GeV}}$ and $\sim 50\%/\sqrt{E_J/\mathrm{GeV}}$, respectively. For any quantitative analysis of the inclusive cross sections, as for the determination of Λ_{QCD}, the absolute calorimetric energy scales have to be known at the per cent level [1,2].

The calibration of the calorimeters at HERA will rely on different methods as: i) calibration of modules in test beams; ii) cross calibration with momentum measurements based on the tracking chambers; iii) utilization of the kinematic peak of the electron energy distribution produced by the dominant small angle scattering of electrons to calibrate the E'_e measurement; iv) internal calibration systems.

Subsequently, we describe another method based on the requirement that neutral current cross sections as measured with electrons, $\sigma_{\mathrm{nc}}^{\mathrm{e}}$, and jets, $\sigma_{\mathrm{nc}}^{\mathrm{J}}$, have to coincide within a given statistical accuracy. The method utilizes the fact that relative shifts of the measured energies,

$$E_e'^{\mathrm{meas}} = E'_e(1 \pm \varepsilon_e),$$
$$E_J^{\mathrm{meas}} = E_J(1 \pm \varepsilon_J), \qquad (1)$$

compared to the original ones give rise to sizeable systematic deviations of these cross sections from the expected behaviour. Striking dependencies occur in different kinematic regions, at low y for the electron and at high y for the jet measurement. The comparison of $\sigma_{\mathrm{nc}}^{\mathrm{e}}$ and $\sigma_{\mathrm{nc}}^{\mathrm{J}}$ in the (x, Q^2) regions which are accessible to both cross section measurements should allow to determine ε_e and ε_J with high statistical precision.

The application of this method to selected (x, Q^2) regions offers therefore interesting possibilities to cross calibrate the measurements of the electromagnetic and hadronic energies against each other. This is of importance since a series of interesting measurements has to be based either on the electron measurement or on the hadron measurement only. For example, the determination of the neutral current structure functions F_2 and F_L at small x will be based essentially on the electron measurement, while for electroweak theory tests the cross section ratio $\sigma_{\mathrm{nc}}^{e^-p}/\sigma_{\mathrm{cc}}^{e^-p}$ will be used, which relies on the jet measurement only. The purpose of this paper is to introduce this method of cross calibration and to illustrate its statistics potential for the case of the H1 detector at HERA.

2. The method

The kinematical variables x, y and Q^2 are determined by the energy and scattering angle of the outgoing electron (E'_e, θ_e) or current jet (E_J, θ_J) as

$$Q_e^2 = 4E_pE'_e \sin^2\left(\frac{\theta_e}{2}\right),$$
$$y_e = 1 - \frac{E'_e}{E_e}\cos^2\left(\frac{\theta_e}{2}\right), \qquad (2)$$
$$Q_J^2 = E_J^2 \sin^2(\theta_J)/(1 - y_J),$$
$$y_J = \frac{E_J}{E_e}\sin^2\left(\frac{\theta_J}{2}\right). \qquad (3)$$

Here, S denotes the cms energy $S = 4E_pE_e$ and $x =$

Q^2/Sy, the angles $\theta_{e(J)}$ are defined with respect to the direction of the electron (proton) beam.

For small angular and energy perturbations $\delta\theta_{e,J}$ and $\delta E_{e,J}/E_{e,J} = \pm\varepsilon_{e,J}$ one derives the corresponding displacements in $x_{e,J}$, $y_{e,J}$ and $Q^2_{e,J}$ as

$$\frac{\delta Q_e^2}{Q_e^2} = \frac{\delta E_e'}{E_e'} \oplus \cot\left(\frac{\theta_e}{2}\right)\delta\theta_e,$$

$$\frac{\delta y_e}{y_e} = \left(1 - \frac{1}{y_e}\right)\frac{\delta E_e'}{E_e'} \oplus \left(1 - \frac{1}{y_e}\right)\tan\left(\frac{\theta_e}{2}\right)\delta\theta_e, \qquad (4)$$

$$\frac{\delta x_e}{x_e} = \frac{1}{y_e}\frac{\delta E_e'}{E_e'} \oplus \left[\cot\left(\frac{\theta_e}{2}\right) - \left(\frac{1}{y_e} - 1\right)\tan\left(\frac{\theta_e}{2}\right)\right]\delta\theta_e \qquad (5)$$

and

$$\frac{\delta Q_J^2}{Q_J^2} = \left(\frac{2 - y_J}{1 - y_J}\right)\frac{\delta E_J}{E_J} \oplus \left[2\cot\theta_J + \frac{y_J}{1 - y_J}\cot\left(\frac{\theta_J}{2}\right)\right]\delta\theta_J,$$

$$\frac{\delta y_J}{y_J} = \frac{\delta E_J}{E_J} \oplus \cot\left(\frac{\theta_J}{2}\right)\delta\theta_J,$$

$$\frac{\delta x_J}{x_J} = \frac{1}{1 - y_J}\frac{\delta E_J}{E_J} \oplus \left[2\cot\theta_J + \frac{2y_J - 1}{1 - y_J}\cot\left(\frac{\theta_J}{2}\right)\right]\delta\theta_J, \qquad (6)$$

with

$$A \oplus B = \sqrt{A^2 + B^2}. \qquad (7)$$

Apart from some specific angular regions the energy uncertainty dominates these relations.

It can be seen that the choice of any two variables $\{a, b\}$ in $d^2\sigma_{nc}/da\,db$ with $\{a, b\} \in \{x, y, Q^2\}$ results in large systematic shifts for small y in the case of the electron measurement and large y in the case of the hadron measurement. In fig. 1 the effect of displacements of $\varepsilon_{e,J}$ on the ratio $(d^2\tilde{\sigma}_{nc}/dx\,dy)/(d^2\sigma_{nc}/dx\,dy)$ is shown illustrating this behaviour. The effect is larger in the case of the electron measurment, which is partly due to the choice of variables. Note, that the ratio $(d^2\tilde{\sigma}_{nc}/dx\,dy)/(d^2\sigma_{nc}/dx\,dy)$ is almost independent of the choice of $\sqrt{S}$.

In the presence of small displacements $\varepsilon_{e,J} \ll 1$ the scattering cross sections $d^2\sigma/dx\,dy$ may be expanded into a Taylor series

$$\frac{d^2\tilde{\sigma}}{dx\,dy}(\varepsilon) = \frac{d^2\tilde{\sigma}}{dx\,dy}(\varepsilon = 0) + \varepsilon\frac{\partial}{\partial\varepsilon}\left[\frac{d^2\tilde{\sigma}}{dx\,dy}\right](\varepsilon = 0) + \varepsilon^2\frac{\partial^2}{2\partial\varepsilon^2}\left[\frac{d^2\tilde{\sigma}}{dx\,dy}\right](\varepsilon = 0) + \cdots, \qquad (8)$$

with $d^2\tilde{\sigma}/dx\,dy(\varepsilon = 0) = d^2\sigma/dx\,dy$. For small values of $\varepsilon_{e,J}$ the cross section ratio $R(x, y)$ is given by

$$R(x, y) = \frac{\dfrac{d^2\tilde{\sigma}}{dx\,dy}(\varepsilon_e)}{\dfrac{d^2\tilde{\sigma}}{dx\,dy}(\varepsilon_J)} = \frac{\sigma_{nc}^{e,meas}}{\sigma_{nc}^{J,meas}} \simeq \frac{1 + \varepsilon_e\delta_e(x, y)}{1 + \varepsilon_J\delta_J(x, y)}. \qquad (9)$$

Our method relies on the observation that the functions $\delta_{e,J}(x, y)$ are independent of $\varepsilon_{e,J}$ and may be determined by Monte Carlo simulations. The calculated functions do only weakly depend on the choice of parameterizations of parton distributions and the inclusion of radiative corrections is straightforward [4,5].

One can rewrite eq. (9) as a linear equation

$$\eta(x, y) = -\varepsilon_J + \xi(x, y)\varepsilon_e + O(\varepsilon^2), \qquad (10)$$

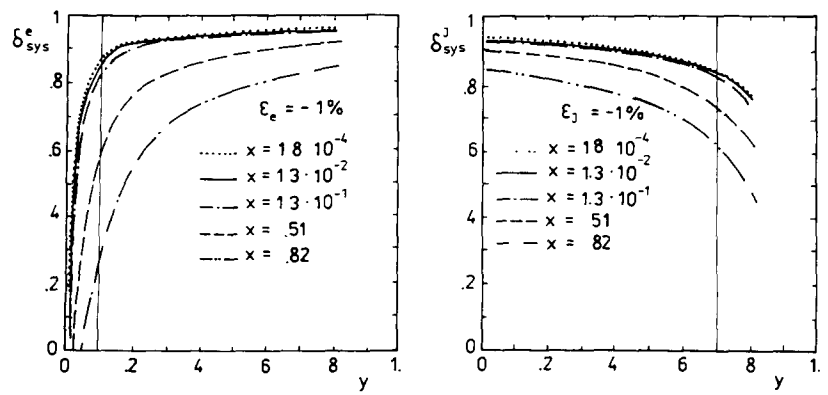

Fig. 1. $\delta_{sys} = (d^2\tilde{\sigma}_{nc}/dx\,dy)/(d^2\sigma_{nc}/dx\,dy)$ for displacements of $\epsilon_{e,J} = -1\%$ with $\dfrac{d^2\tilde{\sigma}}{dx\,dy}(\epsilon) = \dfrac{d^2\sigma}{dx\,dy}(1 + \epsilon)$.

with

$$\eta(x, y) = \frac{R(x, y) - 1}{\delta_J(x, y) R(x, y)},$$

$$\xi(x, y) = \frac{\delta_e(x, y)}{\delta_J(x, y)} \frac{1}{R(x, y)}. \quad (11)$$

The parameters ε_e and ε_J are determined from eq. (10) by a straight line fit using the statistical errors of $\eta(x, y)$ and $\xi(x, y)$. The fit requires to exclude those kinematic regions where either the electron or the hadron cross section is poorly measured. This leads to the following restrictions [1,3]: i) $y \geq 0.1$ because the electron's x resolution varies $\sim 1/y$; ii) $E_J \geq 5$ GeV to enable a hadronic jet measurement; iii) $x \leq 0.7$ to avoid the large smearing corrections at high x and iv) $y \leq 0.8$ because at high y the photoproduction background and radiative corrections become very large and the hadron x resolution grows like $1/(1-y)$.

Performing the fit of eq. (10) in the full kinematic range would in principle yield the values of ε_e and ε_J with high statistical precision even at modest or low luminosities. However, given the complexity and modularity of the big calorimetric detectors it may not be assumed that one must determine just two global parameters ε_e and ε_J only. Instead one has to restrict the electron–hadron comparison to those regions in x and Q^2 which are covered by two specific calorimeters. For the H1 detectors, for example, a particularly interesting case will be to compare cross sections measured with the central barrel hadronic calorimeter CBH and the electromagnetic scintillator calorimeter BEMC, see below. The selection of specific regions of the kinematic plane results in a compromise between luminosity requirements and the width of the (x, Q^2) area considered.

Table 1
Angular ranges of the different calorimeters used in the analysis, see fig. 2

Calorimeter	Angular range	
	Electrons	Hadrons
BEMC	$9° < \theta_e < 25°$	–
BBE	$30° < \theta_e < 34°$	–
CB	$40° < \theta_e < 130°$	$50° < \theta_J < 120°$
FB/IF	$140° < \theta_e < 175°$	
FB/OF		$20° < \theta_J < 40°$
IF		$9° < \theta_J < 15°$
Full hadronic		$9° < \theta_J < 120°$

3. Case study for H1

The H1 detector [6] comprises various types of calorimeters covering different polar angle ranges. This is illustrated in fig. 2 showing a simulated neutral current interaction in the H1 detector. The central tracking chambers see an isolated track in central direction depositing its energy almost completely into the central barrel electromagnetic calorimeter (CBE).

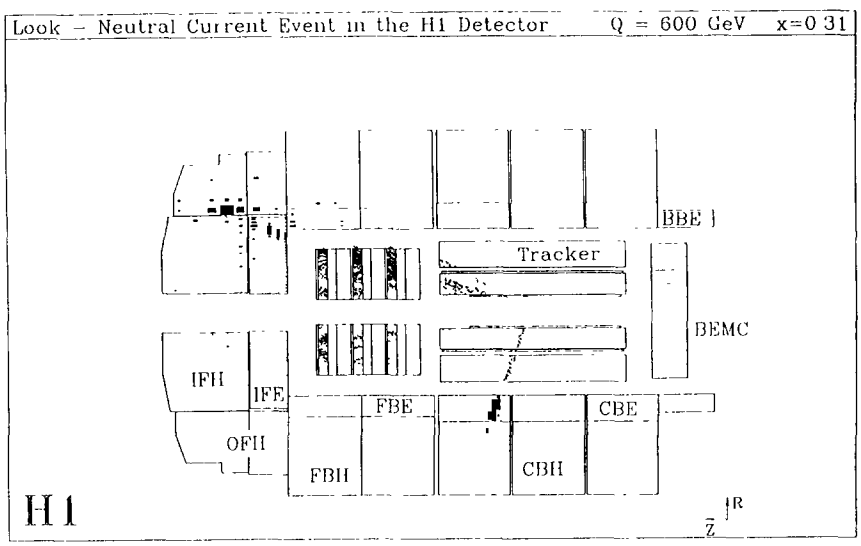

Fig. 2. View of a Monte Carlo neutral current event as seen by the H1 tracking detector and calorimeters. The tracks and energy depositions represent a simulated Monte Carlo event at $Q^2 = 600$ GeV^2 and $x = 0.31$ at the nominal HERA energies $E_e = 30$ GeV and $E_p = 820$ GeV. Nearest to the tracking chamber are electromagnetic calorimeters (BEMC (a lead/scintillator sandwich detector) and the liquid Argon detectors BBE, CBE, FBE and IFE). The outer calorimeters (CBH, OFH and IFH) are situated in the Argon cryostat and measure the hadronic energy [6].

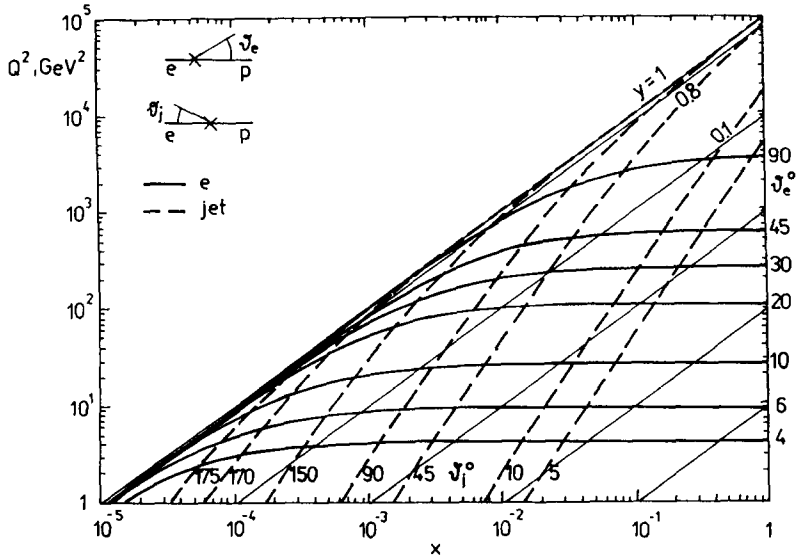

Fig. 3. The (x, Q^2) range explored by HERA experiments at the design beam energies. Lines are drawn of constant polar angle for the scattered electron (solid lines) and the hadronic jet (dashed lines). The deterioration of the electron x resolution restricts the cross calibration to the region of $y \geq 0.1$.

In forward direction a jet is produced with many tracks, the hadronic energy being deposited into the forward hadronic calorimeters IFH and OFH. For the electron–hadron cross section comparison one has to ensure for systematic reasons that all particles belonging to a jet indeed hit the same calorimeter (with small, tolerable losses). This requires to study the opening angle of the hadron jets as functions of (x, Q^2) including fragmentation effects and higher order QCD contributions. According to ref. [7] we have narrowed the angular acceptance of the calorimeters in such a way that more than 70% of the jet energy is contained in the calorimeters. This practically excludes polar angle ranges of about 5° at the edges of the different hadron calorimeters. The angular coverages assumed in the analysis of the various H1 calorimeters are listed in table 1. The (x, Q^2) regions corresponding to specific angular cuts can be read off from fig. 3 showing lines of constant electron angle (solid curves) and average jet angle (dashed ones). It can be easily seen that the restriction to $y \geq 0.1$ as due to the finite electron x and y resolutions, represents a serious constraint to this analysis [#1]. Furthermore it is clear that the higher the Q^2 is the more luminosity will be required to get accurate values for the energy scales ε.

For the simulation of the scattering cross section we used the Born cross section only calculated for the

[#1] Note that the measurements at HERA can be extended to lower y, Q^2 and x if one either measures with electrons and hadrons alone or even combines the measurements [8], e.g., Q_e^2 with y_J [9]. The radiative corrections for the choice Q_e^2, y_J have been calculated recently [5,10].

Table 2
Accuracies of ε_e and ε_J using $d^2\sigma_{nc}/dx\,dy$

electromagnetic calorimeter	hadronic calorimeter	$\mathscr{L}$ [pb^{-1}]	$\sqrt{s}$ = 314 GeV		$\sqrt{s}$ = 190 GeV	
			$\delta\varepsilon_e$	$\delta\varepsilon_J$	$\delta\varepsilon_e$	$\delta\varepsilon_J$
BEMC	CB	10	0.0049	0.0075	0.0050	0.0070
BBE	CB	10	0.0173	0.0220	0.0186	0.0199
CB	CB	10	0.0128	0.0097	0.0130	0.0098
CB	FB/OF	100	0.0158	0.0386	–	–
BEMC	all	10	0.0025	0.0033	0.0026	0.0033
BBE	all	10	0.0073	0.0067	0.0085	0.0068
CB	all	10	0.0031	0.0025	0.0028	0.0025
OF and IF	all	100	0.0258	0.0122	0.0762	0.0324

parametrization of parton distributions DO1 [11] and two sets of energies E_e and E_p. Other choices of parton parametrizations yield similar results, because we consider ratios of cross sections only. Table 2 contains the results from fitting straight lines, as explained above, to the function $\eta(x, y)$ (10). As expected, rather precise determinations appear to be possible from a comparison of the BEMC electron measurement with the CBH hadronic measurement of the cross section. For a luminosity of 10 pb^{-1} one derives errors of ε below 1% for both calorimeters. The other results can be understood as a reflection of the different constraints to the kinematic region (cf. fig. 3). Presently, the luminosity values assumed here appear to be large. However, they have to be reached if precise measurements of the larger Q^2 region shall be performed.

Given the fact that hadronic jets have wide opening angles, sometimes one may even compare the individual electromagnetic calorimeters vs the full liquid argon calorimeter. The resulting statistical errors of ε_e and ε_J are very small (see table 2). There will be systematic effects due to geometry, production and testing sequence, differences in the readout electronics, variations of the magnetic field, cracks, missing channels etc. which potentially affect the method outlined here. Nevertheless, the signature of a genuine miscalibration is striking (fig. 1) and the comparison of the final cross section measurements with electrons and jets must allow at least to set limits to the potential effect of using wrong energy scales. This will be useful in the early stage of the data analysis to detect gross effects and also in the later stage if the systematic error sources become better known and understood.

4. Conclusions

We have presented a method to detect and determine the effect of global miscalibration of electromagnetic and hadron calorimeters at ep colliders comparing neutral current cross sections measured with electrons or hadrons only. The method leads to encouraging results as has been demonstrated for the case of the modular H1 calorimeter system. For example, with a luminosity of 10 pb^{-1} global shifts of the energy scale of the central barrel hadronic calorimeter and the backward electromagnetic calorimeter can be determined to better than 1% as will be necessary for precision measurements and cross section analyses at HERA.

Acknowledgement

We would like to thank J. Feltesse, J. Gayler, K.H. Meier and Th. Naumann for comments and useful discussions.

References

[1] J. Feltesse, in: Proc. of the 1987 HERA Physics Workshop, vol. 1, ed. R.D. Peccei (DESY, Hamburg, 1988) p 33.
[2] J. Blümlein, G. Ingelman, M. Klein and R. Rückl, Z. Phys. C45 (1990) 501.
[3] M. Klein, in: Proc. of the 1990 HERA Physics Workshop, vol. 1, eds. W. Buchmüller and G. Ingelman (DESY, Hamburg 1992) p. 71.
[4] D.Y. Bardin, B. Burdik, P. Christova and T. Riemann, Z. Phys. C42 (1989) 679; H. Spiesberger, DESY 89-175; J. Blümlein, Z. Phys. C47 (1990) 89.
[5] J. Blümlein, Phys. Lett. B271 (1991) 267.
[6] The H1 Collaboration, Technical Proposal, DESY, Hamburg, 1985; F. Brasse, The H1 Detector at HERA, in: Proc. Int. Conf. on High Energy Physics, Dallas, 1992, to appear.
[7] M. Fleischer et al., in: Proc. of the 1990 HERA Physics Workshop, eds. W. Buchmüller and G. Ingelman (DESY, Hamburg 1992) p. 303.
[8] Proc. of the 1990 HERA Physics Workshop, eds. W. Buchmüller and G. Ingelman, (DESY, Hamburg 1992), contributions by C. Hoeger and S. Bentvelsen, J. Engelen, P. Kooijman and G. Bernardi, W. Hildesheim, vol. 1, p. 23, 43, 79.
[9] J. Blümlein and M. Klein, Zeuthen preprint PHE 90-19 (1990); in: Proc. of the 1990 Snowmass Workshop, ed. E. Berger (World Scientific, Singapore, 1992) p. 549.
[10] H. Spiesberger et al., in: Proc. of the 1990 HERA Physics Workshop, vol. 1, eds. W. Buchmüller and G. Ingelman (DESY, Hamburg 1992) p. 101.
[11] D.W. Duke and J.F. Owens, Phys. Rev. D30 (1984) 49.